Crimson Publishers
Wings to the Research

Research Article

Understanding Austenite Microstructural Evolution Under Bar Hot Rolling Conditions for Low and Medium Carbon Steels

Zhang Yongqing[1,2], Felipe Bastos[1,5], J.M Rodriguez-Ibabe[4,5], Beatriz Pereda[4,5]* and Beatriz Lopez[4,5]

[1]China Iron & Steel Research Institute Group, No. 76 Xueyuan Nanlu, Haidian, Beijing 100081, China

[2]Citic Metal Co., Ltd, Room 1901 Capital Mansion Beijing, 100004, China

[3]CBMM, Avenida Brigadeiro Faria Lima, 4285, São Paulo, SP, Brazil

[4]CEIT-Basque Research and Technology Alliance (BRTA), Manuel Lardizabal 15, 20018 Donostia / San Sebastián, Spain

[5]Universidad de Navarra, Tecnun, Manuel Lardizabal 13, 20018 Donostia / San Sebastián, Spain

ISSN: 2576-8840

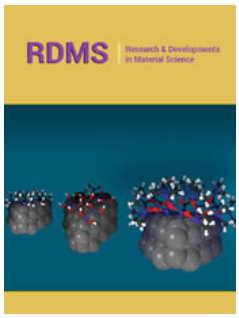

***Corresponding author:** Beatriz Pereda, Universidad de Navarra, Tecnun, Manuel Lardizabal 13, 20018 Donostia / San Sebastián, Spain

Submission: February 03, 2025
Published: February 18 2025

Volume 21 - Issue 3

How to cite this article: Zhang Yongqing, Felipe Bastos, J.M Rodriguez-Ibabe, Beatriz Pereda* and Beatriz Lopez. Understanding Austenite Microstructural Evolution Under Bar Hot Rolling Conditions for Low and Medium Carbon Steels. Res Dev Material Sci. 21(3). RDMS. 001014. 2025.
DOI: 10.31031/RDMS.2025.21.001014

Abstract

Austenite microstructural evolution during flat hot rolling of low carbon steels has been widely investigated, and the role of microalloying elements such as Nb is well established. During hot rolling, Nb retards static softening kinetics, which results in pancaked austenite before phase transformation and in refined room temperature microstructures. However, in bar hot rolling, the carbon contents are usually higher, and during rolling higher strains and strain rates, and much lower interpass times are applied. The role of Nb at these conditions is not so clear. In this work, multipass torsion tests were performed to study the effect of Nb in solid solution or as strain-induced precipitate on the strain accumulation potential under conditions representative of bar hot rolling, with low carbon (0.05%C) and medium carbon steels (0.25%-0.35%C). When the interpass time decreased to 0.5s, dynamic recrystallization was detected in multipass deformation sequences for both Nb and plain carbon steels. Although Nb in solid solution retarded dynamic recrystallization kinetics, strain-induced precipitation did not prevent it. Increasing carbon content did not lead to significant differences in the stress-strain or austenite microstructural evolution mechanisms of the steels. Significant grain refinement of the dynamically recrystallized austenite with Nb microalloying was also observed.

Keywords: Bar hot rolling; Strain-induced precipitation; Strain accumulation; Recrystallization; Austenite microstructural evolution

Introduction

The role of microalloying has been well studied in steel flat products, but not so much in long bar steels. In flat steel production, Nb microalloying is primarily used due to the retardation that it exerts on austenite recrystallization kinetics during austenite hot deformation. This can be due to Nb in solid solution [1], or to Nb(C,N) strain-induced precipitation effects [2,3]. As a result, pancaked austenite microstructures with accumulated strain are obtained before γ→α phase transformation, leading to room temperature microstructural refinement [4,5]. Accordingly, final products with improved mechanical strength and toughness can be achieved [6]. In this context, austenite microstructural evolution models can be useful tools to further

improve Nb efficiency during hot working. In the case of bars and rebars, some works have shown that Nb microalloying results also in improved mechanical properties, due to higher precipitation and grain size hardening [7].

In bar rolling sequences, the strain and strain rates are much higher and the interpass times much shorter than in the case of flat products, which can lead to significant metallurgical differences. At these conditions, the importance of Dynamic Recrystallization (DRX) on the austenite microstructural evolution has been already pointed out [8]. Nonetheless, the information on this topic is scarce, especially for Nb micro alloyed steels. Pussegoda et al. [9] reported that Nb addition can lead to strain accumulation during seamless tube mill rolling. However, the finishing temperatures used in their simulations, in the range of 860ºC, are lower than those encountered under typical bar or rebar rolling conditions. More recent investigations have shown that Nb microalloying, even in low concentrations, can contribute to austenite microstructural homogeneity due to refinement of the reheated austenite microstructure [10,11]. However, the role of Nb microalloying during the hot deformation sequence is still not clear and more information is needed to incorporate these steel compositions into the existing austenite microstructural evolution models. For instance, for low C steels and flat rolling schedules, once strain-induced precipitation starts, static recrystallization is greatly delayed or even suppressed [12,13]. However, when dynamic recrystallization takes place, the role of Nb is not so clear. It has been pointed out that strain-induced precipitates prevent dynamic recrystallization nucleation [8] or that long interpass times are needed to promote a high enough precipitation density [14]. On the other hand, Akben et al. [15] showed that dynamic precipitation during deformation retarded dynamic recrystallization but does not prevent it. However, the strain rates used in their work were much lower than those used during bar hot rolling. In addition, the carbon content of the steels investigated, 0.05%C, is also below those usually employed in bar rolling sequences. Higher carbon contents could also modify strain accumulation behavior, for instance, leading to faster strain-induced precipitation.

The aim of this work is to study these issues. To do so, different types of multipass laboratory torsion tests have been performed with low (0.05%C) and medium carbon (0.25-0.35%C) steels, with and without Nb microalloying additions. The tests were specifically designed to establish the role of Nb solute drag and precipitation effects under bar hot rolling conditions. Multipass deformation schedules (29 passes) more representative of bar hot rolling conditions were also performed.

Materials and Methods

The composition of the steels investigated is detailed in Table 1 (wt%). Three low carbon steels (≅0.05%C), two of them micro alloyed with Nb (0.03%Nb-0.06%Nb), and three medium C steels (0.25-0.35%), two of them also micro alloyed with Nb (0.02%-0.03%Nb) were analyzed.

Table 1: Chemical composition of the steels investigated (in wt%).

Steel	C	Mn	Si	Al	Nb	V	Cr	N
Steel 1, 0.05C	0.05	0.22	0.01	0.05	-	-	-	0.0035
Steel 2, 0.05C-0.03Nb	0.05	0.27	0.02	0.06	0.029		0.03	0.0040
Steel 3, 0.06C-0.06Nb	0.06	1.20	0.29	0.03	0.062	0.05	-	0.0081
Steel 4, 0.35C	0.35	0.75	0.22	0.03	-	-	0.02	0.0026
Steel 5, 0.24C-0.03Nb	0.24	1.25	0.5	-	0.030	0.01	-	0.0056
Steel 6, 0.31C-0.02Nb	0.31	1.04	0.26	-	0.023	-	-	0.0100

Different types of torsion tests were performed. The specimens consisted of a gauge type geometry of 16.5mm in length and 7.5mm in diameter. The thermomechanical cycles applied are shown in Figure 1. Cycles A and B were applied to steels 1, 3, 5 and 6. In these tests, the specimens were first reheated at 1200 ºC for 30min. Next, the roughing step was simulated by applying two deformation passes at high temperature (1100 ºC) with interpass times selected to obtain refined recrystallized austenite microstructures, of ≅40μm, before finishing simulation, calculated with available microstructural evolution models [3,16,17]. After this, in cycle A tests, the specimens were cooled down to 950 ºC, where 8 passes of ε=0.2 with short 0.5s interpass times between them, simulating finishing step, were applied. In the case of cycle B, before application of the 8 finishing passes, an additional pass of ε=0.35 followed by 40s holding time was added. This was done to promote strain-induced precipitation in the Nb micro alloyed steels, and therefore to study its impact on the strain accumulation behavior before application of the final deformation passes. The strain rate was kept constant at $\dot{\varepsilon}=1s^{-1}$ in all passes. After the cycles, the specimens were water quenched for analysis of the resulting austenite microstructures. Compared with low carbon steels for flat products, medium carbon steels are used for rebars with higher pass reduction and higher speed, and shorter interpass time and higher strain rates are obtained.

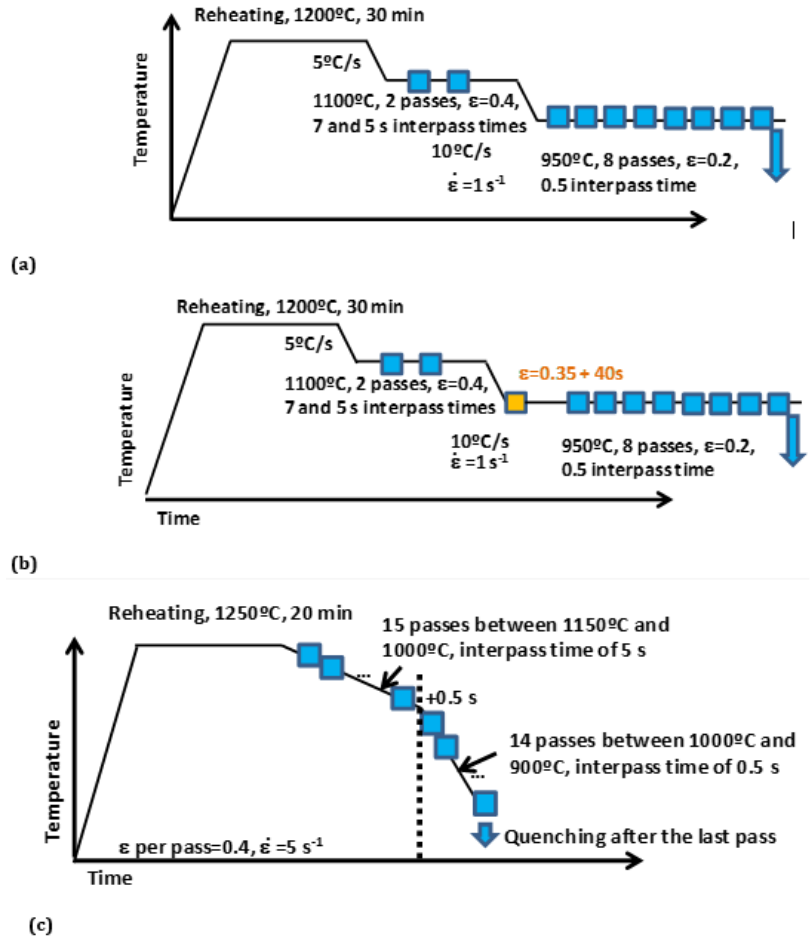

Figure 1: Schemes of the thermomechanical cycles applied in this work: (a) Cycle A, (b) Cycle B, (c) Cycle C.

Cycle C was applied to all the steels investigated. In this case, the aim was to simulate conditions closer to bar hot rolling conditions. Reheating was performed at 1250 ºC for 20min. After this, roughing was simulated by an application of 15 deformation passes with 5s interpass time between them at temperatures from 1150 ºC to 1000 ºC and constant cooling rate, while finishing simulation consisted on 14 deformation passes with 0.5s interpass time between 1000 ºC and 900 ºC. The strain per pass (ε=0.4) and strain rate ($\dot{\varepsilon}$=5s^{-1}) were kept constant. After the cycle, specimens were quenched for austenite microstructure analysis.

Metallographic measurements were carried out on a section corresponding to 0.9 of the outer radius of the torsion specimen, also known as the sub-surface section. Bechet- Beaujard etching [18] was used for revealing the previous austenite grain boundaries in the quenched samples. The etched samples were examined via optical microscopy, and austenite grain size measurements were performed in terms of the Mean Equivalent Diameter (MED). For precipitation analysis, carbon extraction replicas were prepared from quenched specimens and analyzed using a JEM-2100 Transmission Electron Microscope (TEM) operated at 200kV with a LaB6 filament.

Results

Figure 2 shows examples of the stress-strain curves obtained in cycles A and B for steels 1 (0.05C), 3 (0.06C-0.06Nb) and 5 (0.24C-0.03Nb). In all cases, for a given steel composition, the stress levels of the first two deformation passes given at 1100 ºC are similar. With decreasing temperature to 950 ºC an increase in stress is observed. However, after this, the behavior differs depending on steel composition and applied cycle. For the C-Mn steel 1 and cycle A (Figure 1(a)), the stress tends to increase during the first 3 finishing deformation passes up to a peak, then it decreases, and during approximately the three last deformation passes a steady state is reached in the stress levels. This behavior is indicative of strain accumulation during the first deformation passes, and of the activation and completion of dynamic recrystallization during the rest of the sequence [8,9]. For the Nb micro alloyed steels 3 and steel 5, a peak in the stress is also observed during the finishing stages of cycle A. However, the stress increase and decrease are much more gradual, and the strain for reaching the peak stress is clearly retarded for both Nb micro alloyed steels compared to steel. During the last passes, the stress continues to slightly decrease, and the occurrence of steady state is not as clear as in the plain carbon steel.

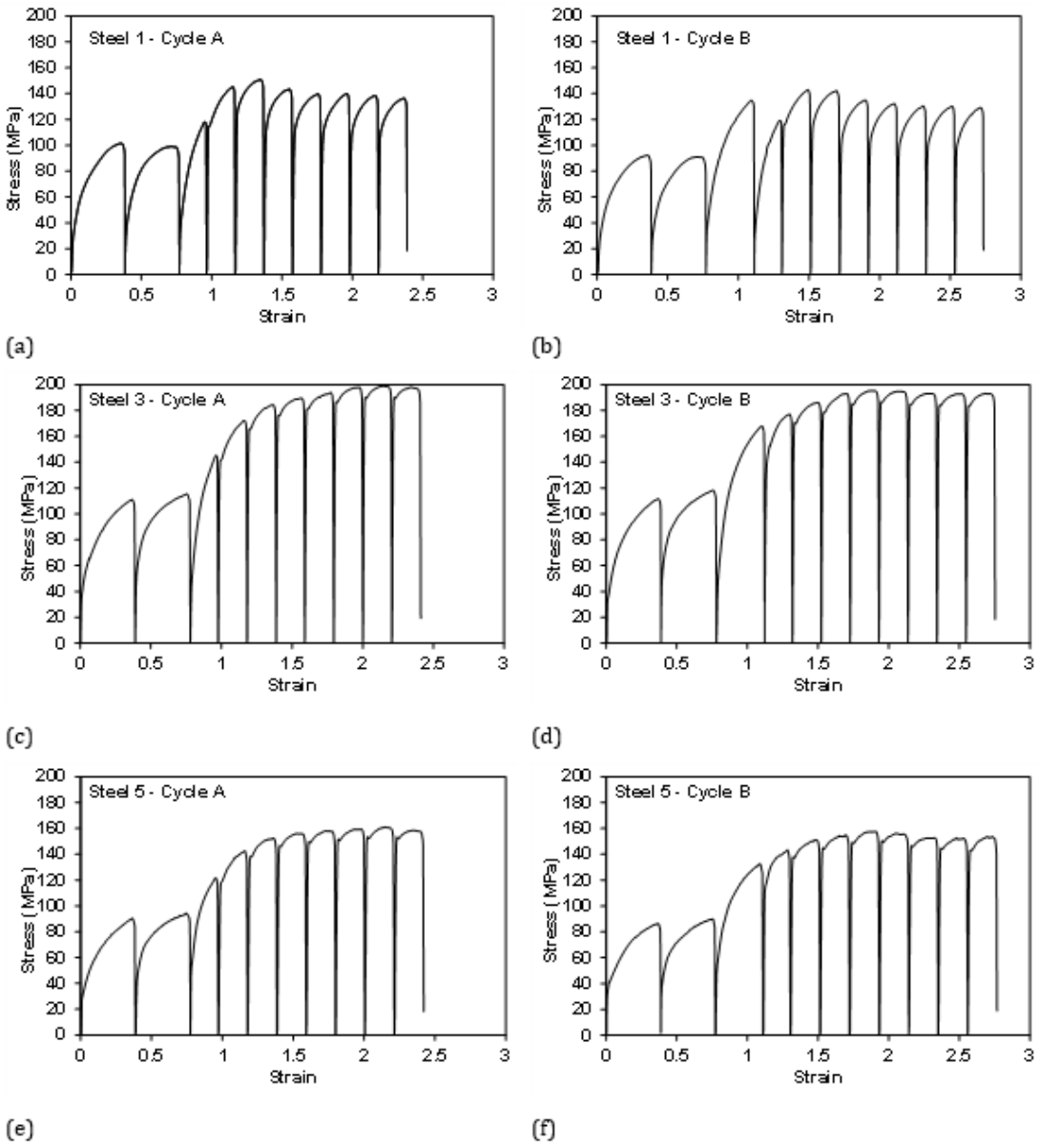

Figure 2: Examples of the stress-strain curves determined for different steels in cycles A and B: (a) Steel 1, 0.05C, cycle A, (b) Steel 1, 0.05C, cycle B, (c) Steel 3, 0.06C-0.06Nb, cycle A, (d) Steel 3, 0.06C-0.06Nb, cycle B, (e) Steel 5, 0.24C-0.03Nb, cycle A, (f) Steel 5, 0.24C-0.03Nb, cycle B.

In cycle B, an additional pass of ε=0.35 followed by a 40s interpass time is added at the start of the finishing stage. For the C-Mn steel, a large stress increase is observed in the third pass due to temperature decrease. However, after 40s holding time, no significant effect of the application of the additional deformation pass is observed and the stress-strain curve is similar to that observed in cycle A, showing the typical shape of dynamic recrystallization activation. On the other hand, for both the low and medium carbon Nb micro alloyed steels (steel 3 and steel 5), while similar stress increase is observed in the third pass due to temperature decrease, during 4th pass, the stress continues to increase. After this, the stress-strain behavior is similar to that observed in cycle A after roughing.

Examples of the austenite microstructures obtained for steel 1 and steel 5 after application of cycle B and quenching are shown in Figure 3. It can be observed that for the C-Mn steel 1, after the test, an equiaxed austenite microstructure was obtained. Since the specimen was quenched just after the application of the last deformation pass, this is in good accordance with the activation of dynamic recrystallization that was detected from the stress-strain curves. On the other hand, for the Nb micro alloyed steel 5, a partially recrystallized microstructure with fine dynamically recrystallized grains coexisting with deformed coarser and elongated unrecrystallized ones was observed. This agrees with the stress-strain behavior (Figure 2(f)) in which stress stabilization that is indicative of dynamic recrystallization steady state regime is not observed for this steel. Significant refinement of the dynamically recrystallized grains compared to the CMn steel can also be noted.

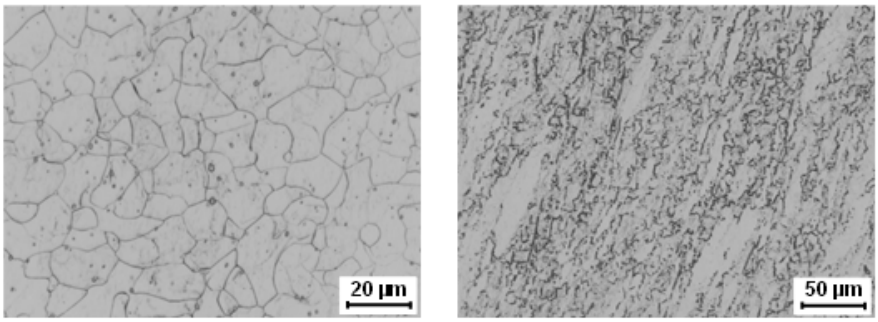

Figure 3: Austenite microstructures obtained for (a) steel 1, 0.05C, and (b) steel 5, 0.24C-0.03Nb, after application of cycle B.

Figure 4 shows examples of precipitates and corresponding EDS analysis obtained from the carbon extraction replicas prepared from the 0.31C-0.02Nb steel 6 after application of cycles A and B. Figure 4(a) shows that after cycle A some precipitates were observed. EDS analysis shows the presence of Nb in their composition (Ni corresponds to the grid holding the replica, and C and N cannot be reliably analyzed in the carbon replicas). However, the particles were scarce and their size suggests that they could be undissolved precipitates remaining during reheating, or scarce strain-induced precipitates that grow during the cycle. Therefore, it can be assumed that most of the Nb present in the composition remains in solid solution during cycle A. On the other hand, after cycle B (Figure 4(b)) a much higher amount of precipitates in the size range of those expected for strain-induced precipitates (5-20nm) [19] was detected. This confirms that application of the additional deformation pass followed by 40s interpass time at 950 ºC results in a significant strain-induced precipitation.

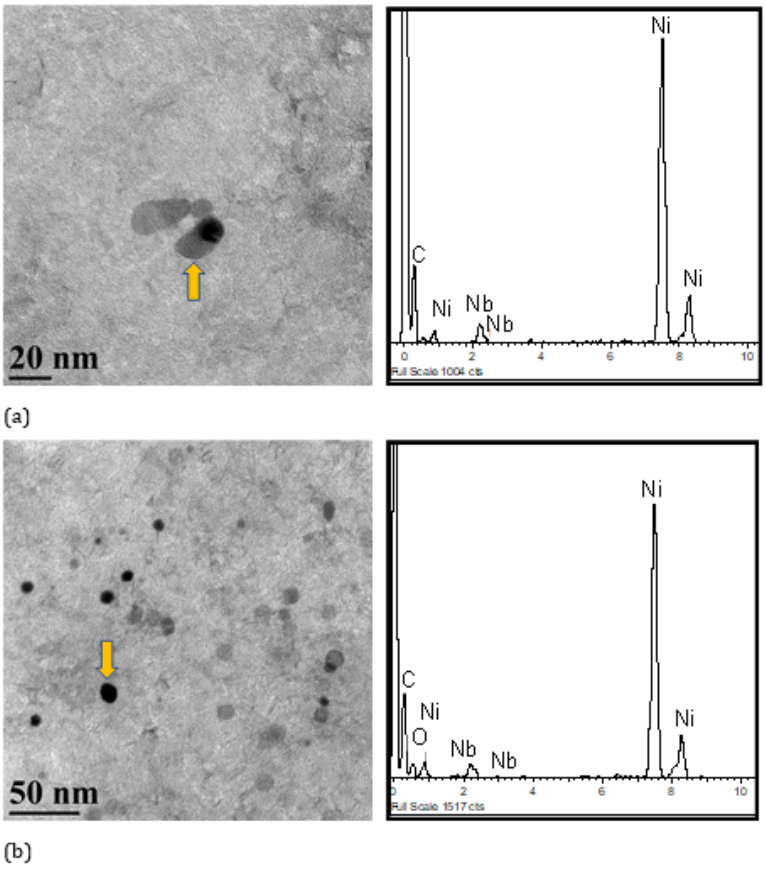

Figure 4: Precipitates detected in the carbon extraction replicas extracted from Steel 6 and examples of EDS analysis of the particles after application of cycles (a) A and (b) B. The arrow in the figures indicates the precipitate in which EDS analysis was performed.

Examples of the stress-strain curves determined for cycle C are shown in Figure 5. For all the steels investigated, the curves show a similar behavior. During the first deformation passes, the stress increases continuously due to temperature decrease. It must be noted that no significant change of stress increase rate was observed for the Nb micro alloyed steels during this stage. After pass 15, when the interpass time decreases from 5 to 0.5s, some increase of the stress levels is observed during the first two finishing deformation passes for all steels investigated. However, in finishing pass 3 for the CMn steels, and during pass 3 and 4 for the Nb micro alloyed steels, some stress decrease is observed. Finally, during the last deformation passes a continuum stress increase is again observed for all the steels. Although the effect of decreasing temperature makes it more difficult to detect, during finishing the stress behavior suggests activation of dynamic recrystallization during finishing simulation.

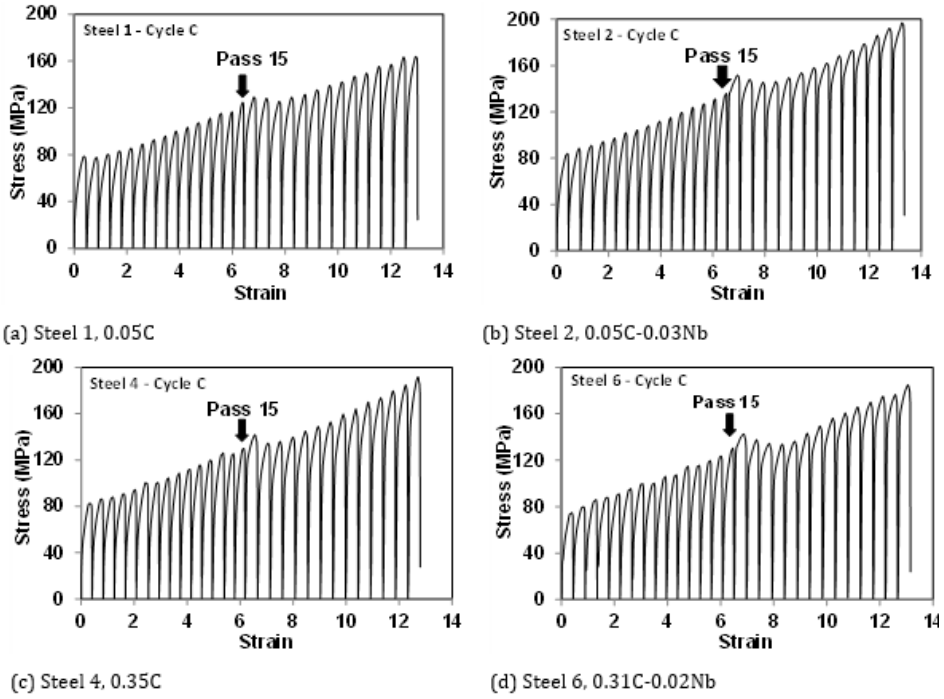

Figure 5: Stress-strain curves obtained for some of the steels investigated after application of cycle C: (a) Steel 1, 0.05C, (b) Steel 2, 0.05C-0.03Nb, (c) Steel 4, 0.35C, (d) Steel 6, 0.31C-0.02Nb.

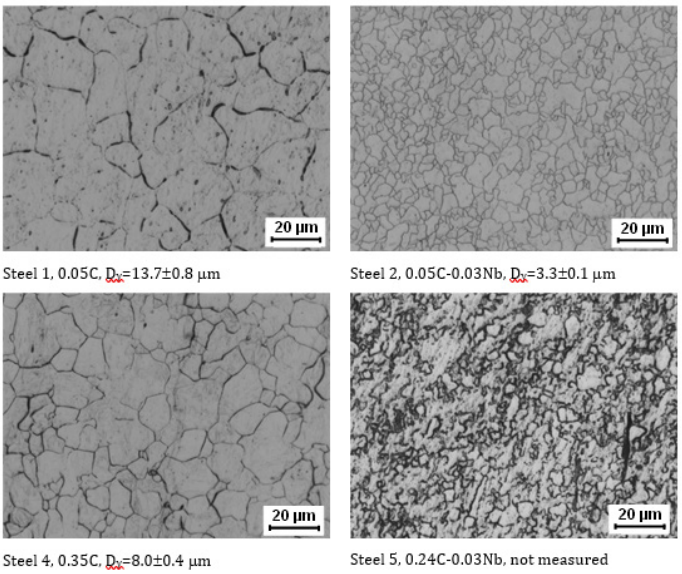

Figure 6: Austenite microstructures obtained after the type C multipass torsion tests for some of the steels investigated.

Examples of the austenite microstructures obtained after the deformation cycle C are shown in Figure 6. It can be observed that in all cases, equiaxed microstructures are obtained for all steels, regardless carbon content or Nb microalloying addition. Since the microstructures were quenched just after application of the last deformation pass, this again supports that dynamic recrystallization is taking place during the final passes of the multipass deformation schedules. However, significant differences can also be observed regarding steel composition. In the range of low carbon (Steels 1 and 2), very large grain size refinement effect can be observed with the addition of Nb, from D_γ=13.7μm to 3.3μm. Some refinement is also observed for the C-Mn steels with increasing carbon content (Steel 1 and 4), from D_γ=13.7μm to 8.0μm. However, although due to the etching quality this was not measured, the finest microstructure was observed for the 0.24C-0.03Nb steel.

Figure 7 shows examples of the precipitates extracted from steel 5 (0.24C-0.03Nb) quenched after application of cycle C. Although not as abundantly as in the case cycle B (Figure 4(b)), the micrograph shows that some fine Nb precipitates could also be found dispersed in this sample, in the size range of that expected for strain-induced precipitates formed during hot deformation [19].

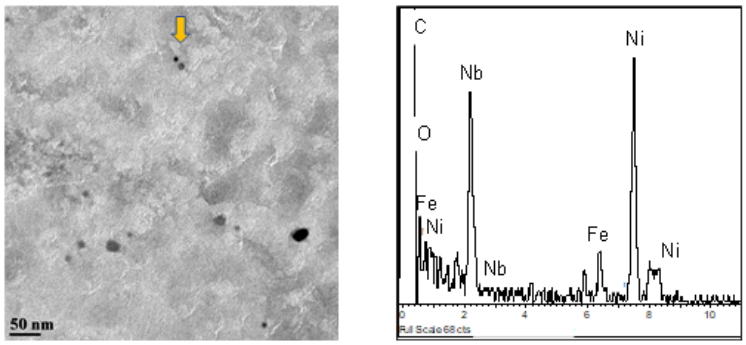

Figure 7: Precipitates observed in steel 5 (0.24C-0.03Nb) quenched after the deformation schedule and corresponding EDS analysis. The arrow in the figure indicates the precipitate in which EDS analysis was performed.

Discussion

Cycles A and B

The austenite microstructural evolution behavior can also be analyzed in terms of the fractional softening (FS) between deformation passes. The following equation is usually employed for fractional softening calculation when double-hit torsion tests are performed [20]:

$$FS = \frac{\sigma_m - \sigma_r}{\sigma_m - \sigma_o} \quad (1)$$

Where σ_m corresponds to the maximum stress level of the first curve, and σ_o and σ_r are the yield stress levels of the curve determined before and after unloading (2% strain offset can be used in the calculations). In cycle A and B, the finishing passes are applied at constant temperature (950 ºC). Therefore, and taking into account that the microstructure after deformation at high temperature (1100 ºC) was fully recrystallized, the softening during finishing passes can be calculated by taking σ_o as the yield strength of the first finishing deformation curve (yield strength of recrystallized austenite with no strain accumulation).

The results obtained for all cycle A and B tests are represented in Figure 8. In the case of cycle A, for all the steels, the interpass softening between the first two finishing deformation passes is very low. This is in concordance with the observed stress increase denoting strain accumulation. Then, after the next deformation passes, the interpass softening remains very low for the Nb micro alloyed steel (<10%) and for the CMn steels, although the softening is slightly larger, it remains below 40% during the rest of the sequence. For both the high and medium carbon Nb micro alloyed steels, the stress-strain curves and microstructural results shown above indicate that DRX is activated for all the steels investigated.

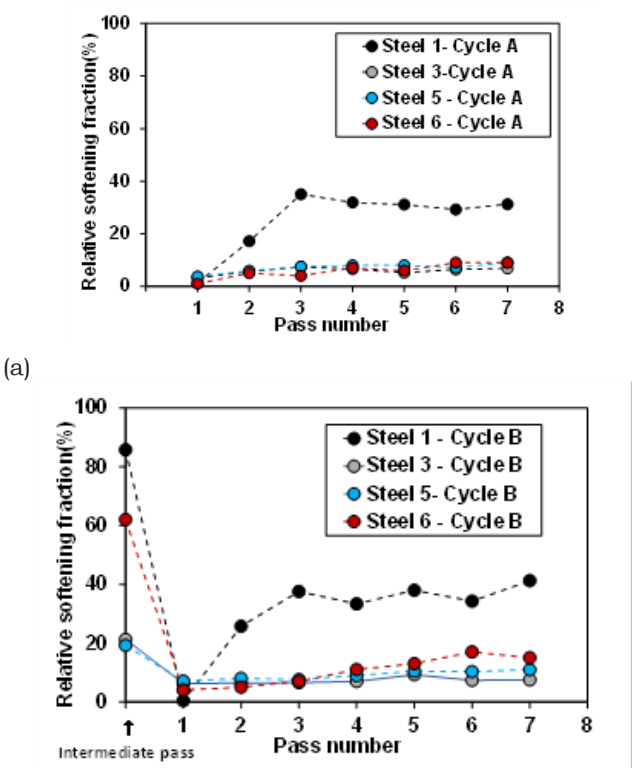

Figure 8: Fractional softening determined for the different steels after application of (a) cycle A and (b) cycle B.

From the stress-strain curves, it can also be observed that both DRX start and progress are significantly retarded for the Nb micro alloyed steels. Since for cycle A no significant precipitation was observed (Figure 4 (a)), it can be concluded that this delay is mainly due to Nb in solid solution, as also reported in other works [15,21]. In addition, this means that, at least during the last deformation passes, post-deformation softening can be mainly attributed to meta dynamic recrystallization (MDRX) [22,23]. MDRX is considered a microstructural evolution mechanism due to growth of the existing DRX nucleus at expenses of the work-hardened grains, provided that a minimum DRX fraction is obtained [24,25]. The low interpass softening values determined for the tests indicate that MDRX evolution during the interpass time is very limited, especially for the Nb micro alloyed steels. This indicates retarding potential of Nb in solid solution on MDRX kinetics.

Larger differences can be observed in the softening behavior in cycle B, Figure 8(b). In this case, after the application of the intermediate deformation pass, different levels of softening are determined for the different steels. For the plain C-Mn steel 1, a high softening level (>85%) is reached. This indicates that, as expected, for this steel recrystallization can progress during the interpass period. On the other hand, for the Nb micro alloyed steels the softening level varies between 60% for steel 6 and about 20% for steels 3 and 5, showing a trend to reduce with increasing Nb content. As usually reported in the literature [3,26], the above results indicate that, for these steels, the occurrence of strain-induced precipitation after the intermediate deformation pass prevents softening. The higher softening level of ≅60% determined for steel 6 can be explained by the combination of lower Nb (0.023%) and higher carbon (0.31%) contents of this steel, which result in the less amount of niobium in solution after reheating. Consequently, retarded strain-induced precipitation kinetics and reduced solute drag effect favors the occurrence of partial recrystallization during the interpass time [2,3,12]. During the final passes, the behavior is similar to that observed in cycle A.

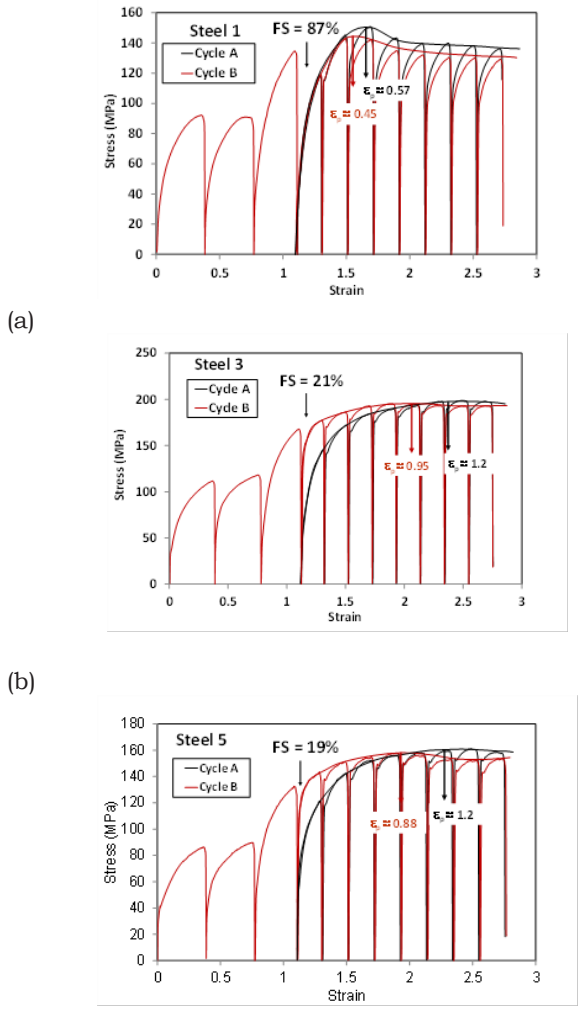

Figure 9: Comparison of finishing deformation curves between cycle A and B for all the tested steels. (a) Steel 1, (b) Steel 3, (c) Steel 5, (d) Steel 6.

To further understand the strain accumulation behavior during the cycles, in Figure 9, the stress-strain curves obtained during the last applied passes are compared for cycles A and B for all steels investigated. To do so, the finishing passes obtained from cycle A have been plotted superimposed on the cycle B curves. Approximate values of the strain for peak stress (ε_p) determined from the finishing curves as well as the softening fraction are also indicated in the figure.

It is interesting to note that for all the steels investigated, lower

ε_p is estimated in cycle B, that is, after application of an additional pass with long 40s interpass time. Although for conventional initial austenite grain size ranges, DRX is reported to start at a critical strain (ε_c) slightly lower than ε_p ($\varepsilon_c=k\cdot\varepsilon_p$ with k<1) [21,23,27], this mainly indicates that dynamic recrystallization start is accelerated by application of this additional pass. However, this can be attributed to different effects depending on steel composition. For the C-Mn steel, the application of a previous deformation pass leads to full recrystallization during the 40 s interpass time (Figure 8(b)), which is expected to result in a refined recrystallized microstructure compared to the initial one. Since dynamic recrystallization is accelerated by reducing the initial grain size [21,28,29], this can explain the observed effect for this steel.

For the Nb micro alloyed steels 2, 3 and 5 after application of the intermediate pass, recrystallization is partially inhibited due to strain-induced precipitation as confirmed by microstructural observations (Figure 4). At these conditions, acceleration of DRX activation can be explained due to the strain accumulation. This is also supported by the shape of the stress-strain curves for the Nb micro alloyed steels, in which an almost continuous stress increase is observed after the application of the first finishing curve in cycle B. However, the pinning effect exerted by strain induced precipitates is not high enough to prevent dynamic recrystallization during subsequent deformation passes with low interpass time between them, regardless of carbon content.

Finally, it should be mentioned that for steel 6, after the 40s interpass time, partial recrystallization takes place. At these conditions, both effects, that is, refinement of the partially recrystallized microstructure and strain accumulation can contribute to the observed DRX kinetics acceleration.

In microstructural evolution models that are applied to multipass deformation schedules, the accumulated strain (ε_{acc}) can be calculated using the following equation:

$$\varepsilon_{acc} = \lambda \cdot (1 - X_{SRX}) \cdot \varepsilon \quad (2)$$

Where X_{SRX} is the recrystallized fraction achieved during the interpass interval and λ is a constant that takes values between λ=0.5 and 1 [30,31]. It is interesting to note that in cycle B for the Nb micro alloyed steels, if the X_{SRX} values calculated after the intermediate pass (X_{SRX} =21%, 19% and 62% for steels 3, 5 and 6, respectively) and a λ value of 1 are used to calculate the ε_{acc}, the values that are determined (ε_{acc} =0.28, 0.28 and 0.13 for steels 3, 5 and 6, respectively), are close to the decrease of the peak strain that it is observed with respect to cycle A ($\Delta\varepsilon_p$ =0.25, 0.32 and 0.18). On the other hand, for the C-Mn steel, the value of ε_{acc} calculated for the CMn steel is much lower than $\Delta\varepsilon_p$ (ε_{acc} =0.045 vs. $\Delta\varepsilon_p$ =0.12), which further supports that in this case grain size refinement would be the main mechanism leading to the ε_p decrease.

Cycle C

In decreasing temperature deformation tests, a modified equation can be applied to calculate the fractional softening between passes [32]:

$$FS = \frac{\sigma_m^i - \sigma_y^{i+1}\dfrac{\sigma_0^i}{\sigma_0^{i+1}}}{\sigma_m^i - \sigma_0^i} \quad (3)$$

Where σ_m^i and σ_y^{i+1} are the maximum and the yield stresses for both, the i-th (at temperature T_i) and the (i+1)st (at temperature T_{i+1}) passes respectively, while σ_0^i and σ_0^{i+1} are the yield stresses of a fully recrystallized material for the i-th and (i+1)st passes. The values of σ_m^i and σ_y^{i+1} are derived from the experimental flow curves, while σ_0^i and σ_0^{i+1} were determined by extrapolation of the yield stresses measured in the stress-strain curves corresponding to the range of complete recrystallization as a function of deformation temperature.

Figure 10 shows the results obtained for all the steels investigated. During the first high temperature passes, where a relatively long interpass time of 5s is applied, full softening takes places for all the steels. Only for the 0.06%Nb micro alloyed steel, this starts to slightly decrease after pass 10 (T=1050 ºC).

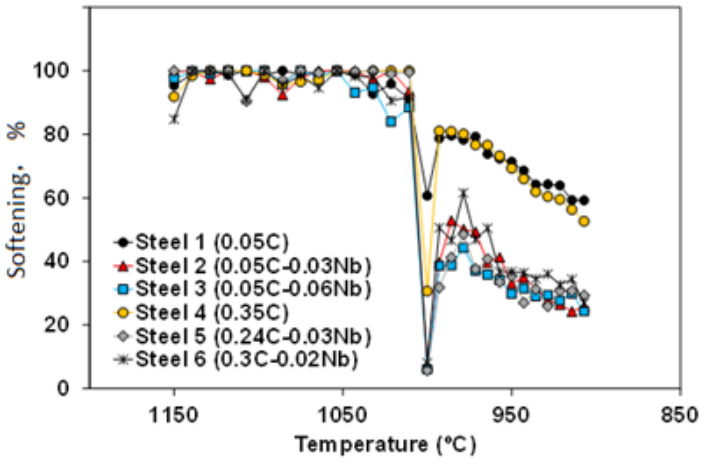

Figure 10: Anisothermal softening kinetics determined in cycle C for the steels investigated.

During multipass deformation at continuous cooling conditions, when strain accumulation starts to occur, a faster increase of stress is usually observed. The temperature at which this happens is defined as the non-recrystallization temperature (T_{nr}). However, in the present tests this behavior is not observed for none of the steels (Figure 5). Conversely, there is a continuous increase of stress during roughing passes. It is well known that the T_{nr} depends on deformation conditions, interpass time and steel composition [33]. No observation of T_{nr} in the present tests can be related to the roughing temperatures applied (1150 ºC-1000 ºC). These temperatures are relatively high compared to the T_{nr} values of ≅1000 ºC and ≅1075 ºC, that were determined in a previous work in tests carried out at similar strain and interpass time conditions, for low carbon 0.03%Nb and 0.06%Nb micro alloyed steels, respectively. This is also in good agreement with the slight softening decrease that it is observed for steel 3 (0.06%Nb) at 1050 ºC. Moreover, slightly lower T_{nr} values could also be expected in the present tests, since the applied strain rates ($\dot{\varepsilon}$ =5s^{-1}) were higher than in reference ($\dot{\varepsilon}$ =1s^{-1}).

When the interpass time decreases to 0.5s, a large softening decrease is observed for all the steels investigated, mainly for the Nb micro alloyed steels. This leads to strain accumulation during the first passes and activation of dynamic recrystallization for all the steels, regardless of Nb or carbon content. During the last passes, lower softening levels are determined for the Nb micro alloyed steels, which indicates meta dynamic recrystallization retardation. This can be mainly attributed to Nb in solid solution [22], although some strain-induced precipitates which can also contribute to this retardation were also observed after the sequences (Figure 7).

Finally, although in these tests stress-strain behavior does not show large differences regarding carbon content, or Nb microalloying addition, it is worth noting the effect that composition exerts on the dynamically recrystallized grains that are obtained after the sequences. While, increasing carbon content results in slight microstructural refinement, larger refinement of the dynamically recrystallized microstructure is observed when Nb is added (Figure 6).

Conclusion

Multipass torsion tests have been performed to investigate the austenite microstructural evolution behavior of low and medium carbon steels, some of them micro alloyed with Nb, under high strain and short interpass time conditions. The main conclusions that can be drawn are:

1. During isothermal multipass deformation tests carried out at low temperature (950 ºC) and short interpass time (0.5s) conditions, for both C-Mn and Nb micro alloyed steels, during the first deformation passes the stress increases due to strain accumulation. However, after a certain number of passes, dynamic recrystallization is activated in all the steels investigated, regardless carbon or niobium content. This was confirmed both by the stress-strain curves and the microstructures observed after the tests.
2. At these conditions, Nb in solid solution leads to significant retardation in the activation and progress of DRX. However, although strain-induced precipitation of niobium carbonitrides can stop static softening, it does not prevent DRX. Moreover, under certain conditions, it can lead to dynamic recrystallization acceleration due to strain accumulation during interpass times and/or to loss of Nb in solid solution owing to precipitation. This behavior was not dependent on carbon content.
3. Activation of DRX was also observed in multipass deformation schedules carried out at decreasing temperature in Nb and C-Mn steels when the interpass time decreased from 5 to 0.5s. At these conditions, the stress-strain curves showed similar behavior regardless of Nb or carbon content, although some retardation of the meta dynamic post-deformation softening was determined for the Nb micro alloyed steels.
4. Some refinement effects of the dynamically recrystallized microstructure was observed with increasing carbon content. However, the effect of Nb microalloying on austenite grain size refinement was found to be much more relevant.

References

1. Andrade AB, Akben HL, Jonas JJ (1983) Effect of molybdenum, niobium, and vanadium on static recovery and recrystallization and on solute strengthening in micro alloyed steels. Met Trans A 14: 1967-1977.
2. Dutta B, Sellars CM (1987) Effect of composition and variables on Nb(C, N) precipitation in niobium micro alloyed austenite. Mater Sci Technol 3: 197-206.
3. Pereda B, Rodriguez-Ibabe JM, Lopez B (2008) Improved model of kinetics of strain induced precipitation and microstructure evolution of Nb micro alloyed steels during multipass rolling. ISIJ Int 48: 1457-1466.
4. Bengochea R, Lopez B, Gutierrez I (1998) Microstructural evolution during the austenite to-ferrite transformation from deformed austenite. Metall Mater Trans A 29: 417-426.
5. Vervynckt S, Verbeken K, Lopez B, Jonas JJ (2013) Modern HSLA steels and role of non-recrystallisation temperature. Int Mater Rev 57: 187-207.
6. Gladman T (1997) The physical metallurgy of micro alloyed steels. Institute of materials, London, UK, pp. 19-78.
7. Hashimoto S, Nakamura M (2006) Effects of microalloying elements on mechanical properties of reinforcing bars. ISIJ Int 46: 1510-1515.
8. Jonas JJ (1994) Dynamic recrystallization - scientific curiosity or industrial tool? Mater Sci Eng A 184: 155-165.
9. Pussegoda LN, Jonas JJ (1991) Comparison of dynamic recrystallization and conventional controlled rolling schedules by laboratory simulation. ISIJ Int 31: 278-288.
10. Jansto SG (2015) Micro Niobium alloy approach in medium and high carbon steel bar, plate and sheet products. Metall Mater Trans B 45: 438-444.
11. Klinkenberg C, Jansto S (2006) Niobium micro alloyed steels for long products. In Proceedings of the International Conference on New Developments in Long and Forged Products: Metallurgy and Applications, Winter Park, United States.
12. Hansen SS, Sande JV, Cohen M (1980) Niobioum carbonitride precipitation and austenite recrystallization in hot-rolled micro alloyed steels. Metall Mater Trans A 11: 387-402.
13. Medina S, Quispe A, Gomez M (2003) Strain induced precipitation effect on austenite static recrystallisation in micro alloyed steels. Mater Sci Technol 19: 99-108.

14. Bowden JW, Samuel FH, Jonas JJ (1991) Effect of interpass time on austenite grain refinement by means of dynamic recrystallization of austenite. Metall Mater Trans A 22: 2947-2957.

15. Akben MG, Bacroix B, Jonas JJ (1983) Effect of vanadium and molybdenum addition on high temperature recovery, recrystallization and precipitation behaviour of niobium-based micro alloyed steels. Acta Metall 31: 161-174.

16. Fernandez AI, Uranga P, Lopez B, Rodriguez-Ibabe JM (2000) Static recrystallization behaviour of a wide range of austenite grain sizes in micro alloyed steels. ISIJ Int 40: 893-901.

17. Pereda B, Aretxabaleta Z, Lopez B (2015) Softening kinetics in high Al and high Al-Nb-micro alloyed steels. J of Mater Eng and Perform 24: 1279-1293.

18. Bechet S, Beaujard L (1955) New reagent for the micro graphical demonstration of the austenite grain of hardened or hardened-tempered steels. Rev Met 52: 5248.

19. Llanos B, Pereda B, Lopez B (2015) Interaction between recovery, recrystallization, and NbC strain-induced precipitation in high-Mn steels. Metall Mat Trans A 46: 5248-5265.

20. Fernandez AI, Lopez B, Rodriguez-Ibabe JM (1999) Relationship between the austenite recrystallized fraction and the softening measured from the interrupted torsion test technique. Scripta Mater 40(5): 543-549.

21. Fernandez AI, Uranga P, Lopez P, Rodriguez-Ibabe JM (2003) Dynamic recrystallization behavior covering a wide austenite grain size range in Nb and Nb-Ti micro alloyed steels. Mat Sci Eng A 361: 367-376.

22. Roucoules C, Yue S, Jonas JJ (1995) Effect of alloying elements on meta dynamic recrystallization in HSLA steels. Metall Mater Trans A 26: 181-190.

23. Siciliano F, Jonas JJ (2000) Mathematical Modeling of the hot strip rolling of micro alloyed Nb, multiply-alloyed Cr-Mo, and plain C-Mn steels. Met Mat Trans A 31: 511-530.

24. Cartmill R, Barnett MR, Zahiri SH, Hodgson PD (2005) An analysis of the transition between strain dependent and independent softening in austenite. ISIJ Int 45: 1903-1908.

25. Uranga P, Fernandez AI, Lopez B, Rodriguez-Ibabe JM (2003) Transition between static and meta dynamic recrystallization kinetics in coarse Nb micro alloyed austenite. Mat Sci Eng A 345: 319-327.

26. Medina SF, Quispe A (2001) Improved model for static recrystallization kinetics of hot deformed austenite in low alloy and Nb/V micro alloyed steels. ISIJ Int 41: 774-781.

27. Poliak EI, Jonas JJ (2003) Initiation of dynamic recrystallization in constant strain rate hot deformation. ISIJ Int 43: 684-691.

28. Sah JP, Richardson GJ, Sellars CM (1974) Grain-size effects during dynamic recrystallization of nickel. Met Sci 8(1).

29. El Wahabi M, Gavard L, Montheillet F, Cabrera JM, Prado JM (2005) Effect of initial grain size on dynamic recrystallization in high purity austenitic stainless steels. Acta Mat 53(17): 4605-4612.

30. Perdrix Ch (1987) Characteristic of plastic deformation of metals during hot working, ECSC Report, No. 7210 EA/31. Institute de Recherches de la Siderurgie Francaise (IRSID), Paris, France.

31. Abad R, Fernandez A, Lopez B, Rodriguez-Ibabe JM (2001) Interaction between recrystallization and precipitation during multipass rolling in a low carbon niobium micro alloyed steel. ISIJ Int 41: 1373-1382.

32. Liu WJ, Akben MG (1987) Softening behaviour of two Ti bearing steels during torsional simulation of rolling. Can Metall Q 26: 145-153.

33. Bai DQ, Yue S, Sun WP, Jonas JJ (1993) Effect of deformation parameters on the no-recrystallization temperature in Nb-Bearing steels. Metallurgical and Materials Transactions A 24: 2151-2159.